
Article:
Liu, Y., Chen, H., Wang, Q. et al. (2 more authors) (2021) Noncircularity-based generalized shift invariance for estimation of angular parameters of incoherently distributed sources. Signal Processing, 183. 107989. ISSN 0165-1684

https://doi.org/10.1016/j.sigpro.2021.107989

Noncircularity-Based Generalized Shift Invariance for Estimation of Angular Parameters of Incoherently Distributed Sources

Yonghong Liu[a,b], Hua Chen[a,b,*], Qing Wang[c], Wei Liu[d], Gang Wang[a]

[a] *Faculty of Electrical Engineering and Computer Science, Ningbo University, Ningbo 315211,P. R. China.*
[b] *Key Laboratory of Intelligent Perception and Advanced Control of State Ethnic Affairs Commission, Dalian 116600, China.*
[c] *School of Electronic Informatin Engineering, Tianjin University, Tianjin 300072, P. R. China.*
[d] *Department of Electronic and Electrical Engineering, University of Sheffield, Sheffield S1 3JD, UK.*

Abstract

In this paper, a reduced-rank angular parameters estimation algorithm is proposed for incoherently distributed (ID) noncircular sources based on a uniform linear array (ULA), which addresses the problems of central direction-of-arrival (DOA) estimation and angular spread estimation. Firstly, the noncircularity property of the signals is utilized to establish an extended generalized array manifold (GAM) model based on the first-order Taylor series approximation. Then, the central DOAs of source signals are obtained based on the generalized shift invariance property of the array manifold and the reduced-rank principle. Next, the angular spreads are estimated from the central moments of the angular distribution. Compared with the existing al-

*Corresponding author
Email addresses: dkchenhua0714@hotmail.com (Hua Chen), wqelaine@tju.edu.cn (Qing Wang), w.liu@sheffield.ac.uk (Wei Liu)

gorithm without exploiting the noncircularity information, the proposed one can achieve a higher accuracy and handle more sources. In addition, it can deal with a general scenario where different sources have different angular distribution shapes. Furthermore, the approximate stochastic Cramer-Rao bound (CRB) of the concerned problem is derived. Simulation results are provided to demonstrate the performance of the proposed algorithm.
Keywords:
Incoherently distributed sources, noncircularity, central DOA estimation, angular spread estimation, generalized shift invariance, rank reduction.

1. Introduction

Direction of arrival (DOA) estimation has developed rapidly over the last few decades, given its wide range of applications such as wireless communication, radar and sonar [1–5]. In most applications, DOA estimation methods are usually developed for the point source model, with the assumption that the signals impinging on the array through one single path. However, in practice, the multipath scattering phenomenon is unavoidable [6–10], which causes angular spread of the impinging source signals, and then affects the signal spatial distribution, making the DOA estimation problem more challenging. Thus, directly applying the classic point-source based multi-signal classification (MUSIC) [11] or ESPRIT types of algorithms [12] in such a scenario will lead to severe performance degradation, or even worse a complete failure of the algorithms. To this end, a spatially distributed source model has been introduced in array signal processing, where two important angular parameters of the received signal are used which are the central DOA and

the angular spread, respectively.

According to the correlation property among different signal paths, one can categorize distributed sources into either coherently distributed (CD) sources or incoherently distributed (ID) sources. For CD sources, as the rank of the noise-free covariance matrix is equal to the number of sources, the dimension of the signal subspace is still equal to the number of sources. Therefore, in the past few decades, parameter estimation of CD sources has been well studied by extending the classic point source methods [13–17]. In [13], in order to estimate the angle parameters of the CD sources, the central DOAs of the sources were firstly estimated using the TLS-ESPRIT algorithm, and then a one-dimensional (1-D) distributed source parameter estimator (DSPE) was constructed for each source to estimate the angular spread. With the assumption of small angular spread, an effective DSPE algorithm [14] and successive DSPE-based algorithm [15] for CD sources were proposed by decoupling the estimation of DOA from that of angular spread of CD sources. In [16], the authors studied the joint estimation of DOA and angular distribution for CD sources in the presence of model errors due to mismatch of the distribution shape between the model and the actual source. In the case of near-field sources and unknown angular distributions, an algorithm was proposed in [17] for jointly estimating the DOA, range, spread angle and shape the CD sources.

However, for ID sources, their components take the entire observation space, leaving the noise subspace empty. As the rank of the noise-free covariance matrix is not equal to the number of sources [6], traditional point source based subspace methods are not applicable in this case. To solve

this problem, the concept of quasi-signal subspace and quasi-noise subspace was introduced [18], and subsequently, a number of effective methods have been studied for DOA estimation of ID sources, such as the dispersed signal parameter estimation (DISPARE) algorithm [18], the maximum likelihood (ML) algorithm [19] and the covariance matching (COMET) algorithm [20]. However, the multidimensional searching operation in [19] leads to an extremely high computational complexity, and to reduce it, a TLS-ESPRIT method was proposed in [13] based on the generalized array manifold (GAM). Although the TLS-ESPRIT method has a lower computational complexity, it has limitations on the structure of the array. In [21], a joint polynomial rooting and general ESPRIT method was proposed for ID source based on a generalized shift invariance property, which is more adaptable in array manifold and has a better performance, and also can handle more ID sources. In the beamspace domain, a shift invariance method was proposed in [22] to efficiently estimate the center DOA and angular spread of the ID sources without the need of spectral peak search. Resorting to the manifold separation technique, a computationally efficient yet accurate estimator [23] was developed for localization of multiple ID sources, which has good applicability for arbitrary array geometries or large angular spreads. In [24], two consecutive one-dimensional searches were performed to decouple the central DOA and the angular spread, and it outperformed the existing algorithms in terms of estimation accuracy and robustness, also the stochastic Cramer-Rao bound (CRB) was derived for the underlying estimation problem.

None of the above work considers the possible noncircular information of the impinging signals, such as the BPSK signal, which has been widely

used in DOA estimation by increasing the array virtual aperture to improve the DOA estimation performance [25–27]. In [28], a method for estimating ID noncircular sources using two closely spaced uniform linear arrays (ULAs) was proposed, which used the cross-correlation matrix to eliminate the influence of noise, and then singular value decomposition (SVD) to obtain the signal subspace for central DOA estimation. In [29], an improved generalized approximate message passing technique was proposed to estimate the central DOA of ID noncircular sources, which is based on sparsity and non-circularity of the signals. However, the methods in [28] and [29] are only focused on center DOA estimation of ID non-circular sources.

In this paper, a novel method for central DOA estimation and angular spread estimation of ID noncircular signals is proposed based on the extended GAM model by using a first-order Taylor series approximation, and combining the generalized shift invariance property and the reduced-rank principle. The contributions of the paper are given as follows.

(1) Compared with Cao's algorithm [21], the proposed algorithm exploits signal noncircularity to handle more ID sources and improves estimation accuracy.

(2) Compared with the multi-dimensional spectrum search method, the proposed algorithm only requires 1-D spectrum search, which reduces the computational complexity.

(3) The proposed algorithm does not require prior knowledge of angular distribution, such that it can be applied to situations where multiple sources have different angular distributions.

The rest of this paper is organized as follows. Section 2 introduces the

general signal model. The proposed algorithm is presented in detail in Section 3. The approximate stochastic CRB of the concerned problem is derived in Section 4. Simulation results are provided in Section 5, followed by conclusions in Section 6.

Notations: $(\cdot)^*$, $(\cdot)^T$, $(\cdot)^{-1}$, $(\cdot)^+$, and $(\cdot)^H$ denote conjugate, transpose, inverse, and conjugate transpose, respectively. $\mathrm{E}\{\cdot\}$ is the expectation operation; $\mathrm{Re}ct[\cdot]$ denotes the rectangular window function; $diag\{\cdot\}$ represents a diagonal matrix formed by its elements; $blkdiag\{\cdot\}$ represents the generation of a block diagonal matrix; $\mathbf{I}_{k\times k}$ is the k-dimensional identity matrix; $\mathbf{0}_{k\times l}$ denotes the $k \times l$ zero matrix; $det\{\cdot\}$ and $tr\{\cdot\}$ denote the determinant and trace of a matrix, respectively; $\lfloor\cdot\rfloor$ is the floor function, giving the largest integer less than or equal to its input; $\otimes$ and $\odot$ are the Kronecker and Hadamard matrix product, respectively; $vec\{\cdot\}$ denotes an operator stacking the columns of a matrix on top of one another; $[\cdot]_{l,k}$ denotes the (l,k)th elements of a matrix.

2. General signal model

Consider a ULA with M elements on the x axis as shown in Fig.1. The distance between adjacent antennas is d which is half-wavelength. It is assumed that there are K uncorrelated narrowband far-field ID noncircular signals $s_k(t), k = 1, 2, \ldots, K$ impinging on the array. The received data vector can be expressed as

$$\mathbf{x}(t) = \sum_{k=1}^{K} s_k(t) \sum_{l=1}^{L_k} \gamma_{k,l}(t)\mathbf{a}(\bar{\theta}_{k,l}) + \mathbf{n}(t) \tag{1}$$

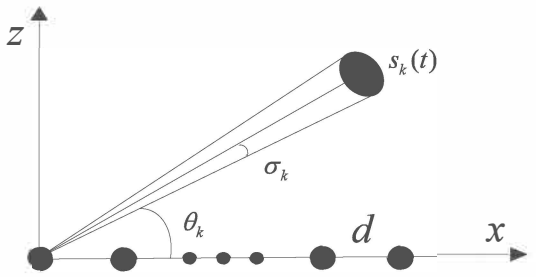

Fig. 1: A uniform linear array structure

where $t = 1, 2, \ldots, T$ is the sampling index, T is the total number of snapshots, L_k is the total number of rays/paths from the kth signal, $\bar{\theta}_{k,l} \in [-90°, 90°]$ is the DOA of the lth ray from the kth signal, with the first antenna as the zero-phase reference point, the array manifold vector $\mathbf{a}(\bar{\theta}_{k,l}) = [1, e^{j2\pi d \sin\bar{\theta}_{k,l}/\lambda}, \cdots, e^{j2\pi(M-1)d\sin\bar{\theta}_{k,l}/\lambda}]^T$, $\gamma_{k,l}(t)$ is the complex-valued path gain, $\mathbf{n}(t) = [n_1(t), \cdots, n_M(t)]^T$ is the $M \times 1$ additive white Gaussian noise vector with zero mean and variance σ_n^2. For ID sources, $\gamma_{k,l}(t)$ is assumed to be temporally white and independent from each other with zero-mean and covariance [21]

$$E\{\gamma_{k,l}(t)\gamma^*_{k',l'}(t')\} = \frac{\sigma^2_{\gamma_k}}{L_k}\delta(k-k')\delta(l-l')\delta(t-t') \tag{2}$$

Angle $\bar{\theta}_{k,l}$ can be represented as

$$\bar{\theta}_{k,l} = \theta_k + \varphi_{k,l}(t) \tag{3}$$

where θ_k is the central DOA of the kth noncircular signal, and $\varphi_{k,l}(t)$ is a small random angular deviation from the central DOA θ_k, which is assumed to be real-valued zero-mean random variables with variance σ_k. Here, we also assume that $\varphi_{k,l}(t)$ is small, and the DOAs from different rays from one noncircular source are relatively close to each other.

It is also assumed that $\zeta \triangleq \varphi_{k,l}(t)$ is a real-valued zero-mean random variable with probability density function $p_k(\zeta;\sigma_k)$. Moreover, $p_k(\zeta;\sigma_k)$ is generally assumed symmetric in terms of ζ. Two typical distributions are the Gaussian distribution and the uniform distribution as given below

$$p_k(\zeta;\sigma_k) = \begin{cases} \frac{1}{\sqrt{2\pi}\sigma_k}\exp\{-0.5\zeta^2/\sigma_k^2\} & \text{Gaussian,} \\ \frac{1}{2\sqrt{3}\sigma_k}\text{Rect}[-\sqrt{3}\sigma_k, \sqrt{3}\sigma_k] & \text{Uniform.} \end{cases} \tag{4}$$

3. The Proposed Method

3.1. Extended GAM Model

According to (3), for a small angle spread, the first-order Taylor series expansion of the manifold vector $\mathbf{a}(\bar{\theta}_{k,l})$ can be approximated as

$$\mathbf{a}(\bar{\theta}_{k,l}) \approx \mathbf{a}(\theta_k) + \mathbf{a}'(\theta_k)\varphi_{k,l}(t) \tag{5}$$

where $\mathbf{a}'(\theta_k)$ is the derivative of $\mathbf{a}(\theta_k)$ with respect to θ_k. Substituting (5) into (1), we have

$$\mathbf{x}(t) \approx \sum_{k=1}^{K} (\mathbf{a}(\theta_k)\upsilon_{k,0}(t) + \mathbf{a}'(\theta_k)\upsilon_{k,1}(t)) + \mathbf{n}(t) \tag{6}$$

where

$$\begin{aligned} \upsilon_{k,0}(t) &= s_k(t)\sum_{l=1}^{L_k}\gamma_{k,l} \\ \upsilon_{k,1}(t) &= s_k(t)\sum_{l=1}^{L_k}\gamma_{k,l}\varphi_{k,l}(t) \end{aligned} \tag{7}$$

Then, we can reformulate (6) into the GAM model as

$$\mathbf{x}(t) \approx \mathbf{B}(\theta)\mathbf{g}(t) + \mathbf{n}(t) \tag{8}$$

where

$$\mathbf{B}(\theta) = [\mathbf{A}(\theta_1), \mathbf{A}(\theta_2), \cdots, \mathbf{A}(\theta_K)] \in C^{M\times 2K} \tag{9}$$

$$\mathbf{A}(\theta_k) = [\mathbf{a}(\theta_k), \mathbf{a}'(\theta_k)] \in C^{M\times 2} \tag{10}$$

$$\mathbf{g}(t) = [\mathbf{g}_1^T, \mathbf{g}_2^T, \cdots, \mathbf{g}_K^T]^T \in C^{2K\times 1} \tag{11}$$

$$\mathbf{g}_k = [\upsilon_{k,0}(t), \upsilon_{k,1}(t)]^T \in C^{2\times 1} \tag{12}$$

It should be noted that the GAM matrix $\mathbf{B}(\theta)$ depends only on the central DOA. Assume that the transmitted signals, the path gains, and the angular deviations are uncorrelated from each other, the variance of $\upsilon_{k,1}(t)$ includes the variance of the angular distribution σ_k^2, that is

$$E\left\{\upsilon_{k,1}(t)\upsilon_{k,1}^*(t)\right\} = \rho_k\sigma_k^2 \tag{13}$$

where $\rho_k = E\left\{|s_k(t)|^2\right\}\sigma_{\gamma_k}^2$ is the power of the kth ID noncircular signal. Additionally, the variance of $\upsilon_{k,0}(t)$ is

$$E\left\{\upsilon_{k,0}(t)\upsilon_{k,0}^*(t)\right\} = \rho_k \tag{14}$$

and the covariance is

$$E\left\{\upsilon_{k,n}(t)\upsilon_{k',n'}^*(t)\right\} = 0, \forall k \neq k' \; or \; n \neq n' \tag{15}$$

From equations (13), (14), and (15), the covariance of $\mathbf{g}(t)$ can be expressed as

$$\mathbf{\Lambda} = E\left\{\mathbf{g}(t)\mathbf{g}^H(t)\right\} = blkdiag\left\{\mathbf{\Lambda}_1, \mathbf{\Lambda}_2, \cdots, \mathbf{\Lambda}_K\right\} \tag{16}$$

where $\mathbf{\Lambda}_k = \rho_k diag\{1, \sigma_k^2\}, k = 1, 2, \cdots, K$.

Here, we consider the case where the received signals are strictly noncircular with the maximal noncircularity rate. Thus, $\mathbf{g}(t)$ can be re-written as [30]

$$\mathbf{g}(t) = \mathbf{\Phi}\mathbf{g}_0(t) \tag{17}$$

where $\mathbf{g}_0(t)$ is a real-valued signal vector, and $\mathbf{\Phi} = diag\{e^{j\omega_1}, e^{j\omega'_1}, \cdots, e^{j\omega_K}, e^{j\omega'_K}\}$ is a $2K \times 2K$ diagonal matrix, whose diagonal elements $\boldsymbol{\omega} = [\omega_1, \omega'_1, \cdots, \omega_K, \omega'_K]^T$ carry the noncircular phase information.

To exploit the noncircularity property of the strictly noncircular signals, a new data vector is constructed by stacking the original data vector $\mathbf{x}(t)$ and its corresponding conjugate counterpart together as follows

$$\begin{aligned}\mathbf{y}(t) &= \begin{bmatrix} \mathbf{x}(t) \\ \mathbf{x}^*(t) \end{bmatrix} = \begin{bmatrix} \mathbf{B}(\theta)\mathbf{g}(t) \\ \mathbf{B}^*(\theta)\mathbf{g}^*(t) \end{bmatrix} + \begin{bmatrix} \mathbf{n}(t) \\ \mathbf{n}^*(t) \end{bmatrix} \\ &= \begin{bmatrix} \mathbf{B}(\theta) \\ \mathbf{B}^*(\theta)\mathbf{\Phi}^{-2} \end{bmatrix} \mathbf{g}(t) + \begin{bmatrix} \mathbf{n}(t) \\ \mathbf{n}^*(t) \end{bmatrix} \\ &= \bar{\mathbf{B}}(\theta)\mathbf{g}(t) + \bar{\mathbf{n}}(t)\end{aligned} \tag{18}$$

where

$$\bar{\mathbf{B}}(\theta) = \begin{bmatrix} \mathbf{B}(\theta) \\ \mathbf{B}^*(\theta)\mathbf{\Phi}^{-2} \end{bmatrix} \in C^{2M \times 2K} \tag{19}$$

is the extended GAM matrix, and $\bar{\mathbf{n}}(t) = \begin{bmatrix} \mathbf{n}(t) \\ \mathbf{n}^*(t) \end{bmatrix} \in C^{2M \times 1}$ is the extended noise matrix.

The covariance matrix of the extended data vector $\mathbf{y}(t)$ is given by

$$\mathbf{R} = E\{\mathbf{y}(t)\mathbf{y}^H(t)\} = \bar{\mathbf{B}}(\theta)\mathbf{\Lambda}\bar{\mathbf{B}}^H(\theta) + \sigma_n^2\mathbf{I}_{2M} \tag{20}$$

where $\mathbf{\Lambda}$ is the convariance matrix of $\mathbf{g}(t)$.

With eigenvalue decomposition (EVD), we have

$$\mathbf{R} = \mathbf{U}_s\mathbf{\Sigma}_s\mathbf{U}_s^H + \mathbf{U}_n\mathbf{\Sigma}_n\mathbf{U}_n^H \tag{21}$$

where the $2M \times 2K$ matrix $\mathbf{U}_s$ is the signal subspace corresponding to diagonal matrix $\mathbf{\Sigma}_s$ composed of the $2M$ largest eigenvalues, and the $2M \times (2M -$

$2K$) matrix $\mathbf{U}_n$ is the noise subspace corresponding to diagonal matrix $\mathbf{\Sigma}_n$ composed of the $(2M-2K)$ smallest eigenvalues.

3.2. Central DOA Estimation

The sensor array is first divided into two subarrays, each with $N = M-1$ sensors. They include sensors $\{x_1, \cdots, x_{M-1}\}$ and $\{x_2, \cdots, x_M\}$, respectively. For simplicity, $\{x_{1,n}\}_{n=1}^{N}$ and $\{x_{2,n}\}_{n=1}^{N}$ are used to represent the locations of the sensors in each subarray, where $x_{1,n} < x_{2,n}, n = 1, \cdots, N$.

Define the following selection matrix

$$\mathbf{J}_1 = [\ \mathbf{I}_{N\times N} \quad \mathbf{0}_{N\times 1}\ ] \in C^{N\times M} \tag{22}$$

$$\mathbf{J}_2 = [\ \mathbf{0}_{N\times 1} \quad \mathbf{I}_{N\times N}\ ] \in C^{N\times M} \tag{23}$$

According to (9), (10) and (19), we have

$$\mathbf{K}_2\bar{\mathbf{a}}(\theta_k) = \mathbf{\Omega}_k\mathbf{K}_1\bar{\mathbf{a}}(\theta_k) \tag{24}$$

$$\mathbf{K}_2\bar{\mathbf{a}}'(\theta_k) = \mathbf{\Omega'}_k\mathbf{K}_1\bar{\mathbf{a}}'(\theta_k) \tag{25}$$

where

$$\bar{\mathbf{a}}(\theta_k) = \begin{bmatrix} \mathbf{a}(\theta_k) \\ e^{-j2\omega_k}\mathbf{a}^*(\theta_k) \end{bmatrix} \in C^{2M\times 1} \tag{26}$$

$$\bar{\mathbf{a}}'(\theta_k) = \begin{bmatrix} \mathbf{a}'(\theta_k) \\ e^{-j2\omega'_k}\mathbf{a}'^*(\theta_k) \end{bmatrix} \in C^{2M\times 1} \tag{27}$$

$$\mathbf{\Omega}_k = blkdiag\{e^{j\phi_k}\mathbf{I}_{N\times N}, e^{-j\phi_k}\mathbf{I}_{N\times N}\}, \phi_k = 2\pi d\sin\theta_k/\lambda \tag{28}$$

$$\mathbf{\Omega'}_k = diag\{\beta_1 e^{j\phi_k}, \cdots, \beta_N e^{j\phi_k}, \beta_1 e^{-j\phi_k}, \cdots, \beta_N e^{-j\phi_k}\} \in C^{2N\times 2N}, \beta_n = \frac{x_{2,n}}{x_{1,n}}, \tag{29}$$

where $\mathbf{a}(\theta_k)$ is an $M \times 1$ vector whose mth element is $e^{j2\pi(m-1)d\sin\theta_k/\lambda}$; $\mathbf{a}'(\theta_k)$ is the derivative of $\mathbf{a}(\theta_k)$ with respect to θ_k; $\mathbf{a}^*(\theta_k)$ and $\mathbf{a}'^*(\theta_k)$ are the conjugates of $\mathbf{a}(\theta_k)$ and $\mathbf{a}'(\theta_k)$, respectively; $\mathbf{K}_1 = blkdiag\{\mathbf{J}_1, \mathbf{J}_1\}$, and $\mathbf{K}_2 = blkdiag\{\mathbf{J}_2, \mathbf{J}_2\}$. From (24) and (25), we have

$$\bar{\mathbf{B}}(\theta_k) = [\bar{\mathbf{a}}(\theta_k), \bar{\mathbf{a}}'(\theta_k)] \tag{30}$$

$$\mathbf{K}_2\bar{\mathbf{B}}(\theta) = [\mathbf{\Omega}_1\mathbf{K}_1\bar{\mathbf{a}}(\theta_1), \mathbf{\Omega'}_1\mathbf{K}_1\bar{\mathbf{a}}'(\theta_1)\cdots, \mathbf{\Omega}_K\mathbf{K}_1\bar{\mathbf{a}}(\theta_K), \mathbf{\Omega'}_K\mathbf{K}_1\bar{\mathbf{a}}'(\theta_K)]. \tag{31}$$

Clearly, $\mathbf{U}_s$ has the same column space as the GAM matrix $\bar{\mathbf{B}}(\theta)$, which yields

$$\mathbf{U}_s = \bar{\mathbf{B}}(\theta)\mathbf{T} \tag{32}$$

where $\mathbf{T}$ is an invertible $2K \times 2K$ matrix.

We can extract two submatrices $\mathbf{U}_1$ and $\mathbf{U}_2$ from $\mathbf{U}_s$ whose rows correspond to the partition of the two subarrays, where $\mathbf{U}_1, \mathbf{U}_2 \in C^{2N\times 2K}$. Then, we have

$$\mathbf{U}_1 = \mathbf{K}_1\bar{\mathbf{B}}(\theta)\mathbf{T} \tag{33}$$

$$\mathbf{U}_2 = \mathbf{K}_2\bar{\mathbf{B}}(\theta)\mathbf{T} \tag{34}$$

Define a new matrix $\mathbf{\Psi}(\theta)$ as

$$\mathbf{\Psi}(\theta) = blkdiag\{e^{j\psi}\mathbf{I}_{N\times N}, e^{-j\psi}\mathbf{I}_{N\times N}\} \tag{35}$$

where $\psi = 2\pi d\sin\theta/\lambda$. Then we construct $\mathbf{D}(\theta)$ as

$$\mathbf{D}(\theta) = \mathbf{U}_2 - \mathbf{\Psi}(\theta)\mathbf{U}_1 = (\mathbf{K}_2\bar{\mathbf{B}} - \mathbf{\Psi}(\theta)\mathbf{K}_1\bar{\mathbf{B}})\mathbf{T} = \mathbf{Q}(\theta)\mathbf{T} \tag{36}$$

where $\mathbf{Q}(\theta) = (\mathbf{K}_2\bar{\mathbf{B}} - \mathbf{\Psi}(\theta)\mathbf{K}_1\bar{\mathbf{B}})$. Using (31), $\mathbf{Q}(\theta)$ can be rewritten as

$$\begin{aligned}\mathbf{Q}(\theta) = [&(\mathbf{\Omega}_1 - \mathbf{\Psi}(\theta))\,\mathbf{K}_1\bar{\mathbf{a}}(\theta_1), (\mathbf{\Omega'}_1 - \mathbf{\Psi}(\theta))\,\mathbf{K}_1\bar{\mathbf{a}}'(\theta_1), \cdots, \\ &(\mathbf{\Omega}_K - \mathbf{\Psi}(\theta))\,\mathbf{K}_1\bar{\mathbf{a}}(\theta_K), (\mathbf{\Omega'}_K - \mathbf{\Psi}(\theta))\,\mathbf{K}_1\bar{\mathbf{a}}'(\theta_K)]\end{aligned} \tag{37}$$

It can be seen from (37) that when $\theta = \theta_k$, all the elements of $(\mathbf{\Omega}_k - \mathbf{\Psi}(\theta))$ become zero. Therefore, if $K \leq N$, then $\mathbf{D}(\theta)$ is rank deficient and the determinant of $\mathbf{D}^H(\theta)\mathbf{D}(\theta)$ is zero. The estimated value $\{\hat{\theta}_k\}_{k=1}^K$ of the noncircular signals central DOA can be obtained by searching for the peaks of the following function

$$f(\theta) = \frac{1}{\det\{\mathbf{D}^H(\theta)\mathbf{D}(\theta)\}} \tag{38}$$

3.3. Angular Spread Estimation

From (20), $\mathbf{\Lambda}$ can be estimated as

$$\hat{\mathbf{\Lambda}} = \bar{\mathbf{B}}(\hat{\theta})^+(\hat{\mathbf{R}} - \hat{\sigma}_n^2\mathbf{I}_{2M})(\bar{\mathbf{B}}^H(\hat{\theta}))^+ \tag{39}$$

where $\bar{\mathbf{B}}(\hat{\theta})$ is the estimate of $\bar{\mathbf{B}}(\theta)$ by substituting the estimates of θ into (19). Furthermore, the estimate of the variance $\hat{\sigma}_n^2$ of the noise can be calculated by the average of the $(2M - 2K)$ smallest eigenvalues of $\hat{\mathbf{R}}$. According to the expression of $\mathbf{\Lambda}$ in (16), the angular spreads can be given by

$$\hat{\sigma}_k = \sqrt{\frac{1}{2}\left(\frac{[\hat{\mathbf{\Lambda}}]_{2k,2k}}{[\hat{\mathbf{\Lambda}}]_{2k-1,2k-1}} + \frac{[\hat{\mathbf{\Lambda}}]_{2K+2k,2K+2k}}{[\hat{\mathbf{\Lambda}}]_{2K+2k-1,2K+2k-1}}\right)}, \quad k = 1, 2, \cdots, K \tag{40}$$

The proposed algorithm for estimating the angular parameters of incoherently distributed noncircular sources is summarized in Table 1.

4. The approximate Cramer-Rao bound

To derive the approximate stochastic CRB of the concerned problem, we first define a vector $\boldsymbol{\eta}$ containing all the interesting parameters as

$$\boldsymbol{\eta} = [\boldsymbol{\mu}^T, \boldsymbol{\upsilon}^T]^T \in C^{(4K+1)\times 1} \tag{41}$$

Table 1: Summary of the proposed algorithm.

Algorithm: Estimation of the central DOA and the angular spreads of ID noncircular sources.
Step 1 Obtain the extended data vector $\mathbf{y}(t)$ according to (18).
Step 2 Calculate the covariance matrix $\hat{\mathbf{R}}$ via (20), and perform EVD on $\hat{\mathbf{R}}$ to obtain $\hat{\mathbf{U}}_s$.
Step 3 Extract two submatrices $\mathbf{U}_1$ and $\mathbf{U}_2$ from $\mathbf{U}_s$, and formulate matrix $\mathbf{D}_\theta$.
Step 4 Estimate the central DOAs through peak search of (38).
Step 5 Calculate $\hat{\mathbf{\Lambda}}$ via (39) and estimate the angular spreads with (40).

where $\boldsymbol{\mu} = [\boldsymbol{\theta}^T, \boldsymbol{\sigma}^T]^T \in C^{2K\times 1}$ with the central DOAs $\boldsymbol{\theta} = [\theta_1, \theta_2, \cdots, \theta_K]^T$ and the angle spreads $\boldsymbol{\sigma} = [\sigma_1, \sigma_2, \cdots, \sigma_K]^T$, $\boldsymbol{\upsilon} = [\boldsymbol{\psi}^T, \boldsymbol{\rho}^T, \sigma_n^2]^T \in C^{(2K+1)\times 1}$ with the noncircular phases $\boldsymbol{\psi} = [\varphi_1, \varphi_2, \cdots, \varphi_K]^T$ and $\boldsymbol{\rho} = [\rho_1, \rho_2, \cdots, \rho_K]^T$.

Under the assumption of small angular spreads, the conjugated and unconjugated covariance matrix $\mathbf{R}_1$ and $\mathbf{R}_1'$ of the observation can be approximated as [21], respectively

$$\mathbf{R}_1 \approx \sum_{k=1}^{K} \rho_k \mathbf{R}_s(\theta_k, \sigma_k) + \sigma_n^2 \mathbf{I}_M \tag{42}$$

$$\mathbf{R'}_1 \approx \sum_{k=1}^{K} \rho_k e^{j\varphi_k} \mathbf{R'}_s(\theta_k, \sigma_k) \tag{43}$$

where $\mathbf{R}_s(\theta_k, \sigma_k) = \mathbf{a}(\theta_k)\mathbf{a}^H(\theta_k) \odot \mathbf{G}(\theta_k, \sigma_k)$ and $\mathbf{R'}_s(\theta_k, \sigma_k) = \mathbf{a}(\theta_k)\mathbf{a}^T(\theta_k) \odot \mathbf{G}'(\theta_k, \sigma_k)$. $\mathbf{G}(\theta_k, \sigma_k)$ is a Toeplitz matrix with the (p, q)th element given by

$$[\mathbf{G}(\theta_k, \sigma_k)]_{p,q} = \begin{cases} \sin c\left((2\sqrt{3}\sigma_k(x_p - x_q)\cos\theta_k)/\lambda\right) \text{ Uniform,} \\ \exp\left(-(\frac{2\pi}{\lambda}(x_p - x_q)\sigma_k \cos\theta_k)^2/2\right) \text{ Gaussian,} \end{cases}$$

and $\mathbf{G}'(\theta_k, \sigma_k)$ is an anti-Toeplitz matrix with the (p,q)th element given by

$$[\mathbf{G}'(\theta_k, \sigma_k)]_{p,q} = \begin{cases} \sin c\left((2\sqrt{3}\sigma_k(x_p+x_q-2)\cos\theta_k)/\lambda\right) \text{ Uniform,} \\ \exp\left(-(\frac{2\pi}{\lambda}(x_p+x_q-2)\sigma_k\cos\theta_k)^2/2\right) \text{ Gaussian.} \end{cases}$$

Considering the noncircularity of the incoming signals, the extended covariance matrix $\mathbf{R}$ can be further rewritten as

$$\mathbf{R} = \begin{bmatrix} \mathbf{R}_1 & \mathbf{R}'_1 \\ \mathbf{R}'^*_1 & \mathbf{R}^*_1 \end{bmatrix} \tag{44}$$

The CRB of $\boldsymbol{\eta}$ can be calculated as [24, 30]

$$CRB(\boldsymbol{\eta}) = \mathbf{F}^{-1} \tag{45}$$

where $\mathbf{F}$ is the Fisher information matrix (FIM) with the (p,q)th entry defined as

$$[\mathbf{F}]_{p,q} = \frac{T}{2} tr\left\{\mathbf{R}^{-1}\frac{\partial \mathbf{R}}{\partial \eta_p}\mathbf{R}^{-1}\frac{\partial \mathbf{R}}{\partial \eta_q}\right\} \tag{46}$$

Furthermore, (46) can be rewritten as

$$\frac{2}{T}\mathbf{F} = \left(\frac{\partial \mathbf{h}}{\partial \boldsymbol{\eta}^T}\right)^H \left(\mathbf{R}^{-T} \otimes \mathbf{R}^{-1}\right)\left(\frac{\partial \mathbf{h}}{\partial \boldsymbol{\eta}}\right) \tag{47}$$

where $\mathbf{h} = vec\{\mathbf{R}\}$.

With the partition

$$\left(\mathbf{R}^{-T/2} \otimes \mathbf{R}^{-1/2}\right)\left[\frac{\partial \mathbf{h}}{\partial \boldsymbol{\mu}^T}\middle|\frac{\partial \mathbf{h}}{\partial \boldsymbol{\upsilon}^T}\right] \triangleq [\mathbf{U}\,|\mathbf{V}] \tag{48}$$

where

$$\mathbf{U} = \left(\mathbf{R}^{-T/2} \otimes \mathbf{R}^{-1/2}\right)\left[\frac{\partial \mathbf{h}}{\partial \boldsymbol{\theta}^T}\middle|\frac{\partial \mathbf{h}}{\partial \boldsymbol{\sigma}^T}\right] = [\mathbf{U}_\theta\,|\mathbf{U}_\sigma] \tag{49}$$

$$\mathbf{V} = \left(\mathbf{R}^{-T/2} \otimes \mathbf{R}^{-1/2}\right)\left[\frac{\partial \mathbf{h}}{\partial \boldsymbol{\varphi}^T}\middle|\frac{\partial \mathbf{h}}{\partial \boldsymbol{\rho}^T}\middle|\frac{\partial \mathbf{h}}{\partial \sigma_n^2}\right] = [\mathbf{U}_\psi\,|\mathbf{V}_s\,|\mathbf{V}_n] \tag{50}$$

where the kth column of $\mathbf{U}_\theta$, $\mathbf{U}_\sigma$, $\mathbf{U}_\psi$, $\mathbf{V}_s$ and $\mathbf{V}_n$ are as follows

$$\mathbf{U}_\theta(:,k) = vec\left\{\mathbf{R}^{-1/2}\frac{\partial \mathbf{R}}{\partial \theta_k}\mathbf{R}^{-1/2}\right\} \tag{51}$$

$$\mathbf{U}_\sigma(:,k) = vec\left\{\mathbf{R}^{-1/2}\frac{\partial \mathbf{R}}{\partial \sigma_k}\mathbf{R}^{-1/2}\right\} \tag{52}$$

$$\mathbf{U}_\psi(:,k) = vec\left\{\mathbf{R}^{-1/2}\frac{\partial \mathbf{R}}{\partial \varphi}\mathbf{R}^{-1/2}\right\} \tag{53}$$

$$\mathbf{V}_s(:,k) = vec\left\{\mathbf{R}^{-1/2}\frac{\partial \mathbf{R}}{\partial \rho_k}\mathbf{R}^{-1/2}\right\} \tag{54}$$

$$\mathbf{V}_n(:,k) = vec\left\{\mathbf{R}^{-1/2}\frac{\partial \mathbf{R}}{\partial \sigma_n^2}\mathbf{R}^{-1/2}\right\} \tag{55}$$

Then we can rewrite (47) as

$$\frac{2}{T}\mathbf{F} = \begin{bmatrix} \mathbf{U}^H \\ \mathbf{V}^H \end{bmatrix} [\ \mathbf{U} \quad \mathbf{V}\ ] \tag{56}$$

Resorting to the block matrix inversion lemma [30] by taking the upper-left corner of $\mathbf{F}^{-1}$, we can attain the interesting angle parameters $CRB(\boldsymbol{\mu})$ from (45).

Remark 1: The major computational effort of the proposed algorithm includes the construction of $\hat{\mathbf{R}}$, performing EVD on $\hat{\mathbf{R}}$, spectral searching and Step 5. Denote the number of searches for estimating the central DOAs by Δ. To calculate $\hat{\mathbf{R}}$ and perform EVD on $\hat{\mathbf{R}}$, a computational complexity of $O((2M)^2T)$ and $O((2M)^3)$ is needed, respectively. The complexity for 1D spectral search of Step 4 is about $O(\Delta(8NK^2 + 16N^2K))$. The complexity of Step 5 is $O(8MK^2 + 2(2M)^2K)$. The total computational complexity of the proposed algorithm is about $O((2M)^2T + (2M)^3 + \Delta(8NK^2 + 16N^2K) + 8MK^2 + 2(2M)^2K)$.

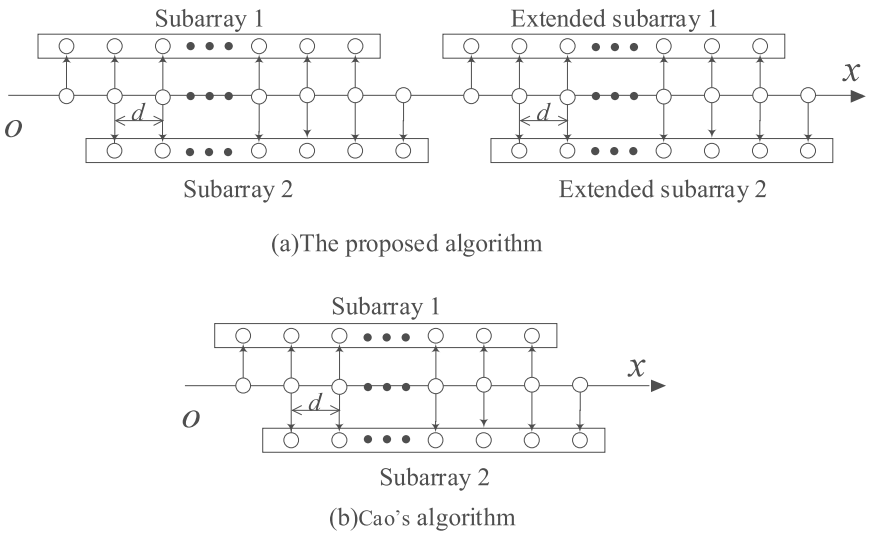

Fig. 2: Subarray selection of the proposed algorithm and Cao's algorithm.

Remark 2: Compared to Cao's algorithm in [21], the proposed method exploits the additional information provided by noncircular signals by extending the virtual array aperture. The maximum number of distinguishable signals by the proposed algorithm is based on the new extended data vector in (18) as well as the matrix $\mathbf{D}(\theta)$ in (36), which is shown in Fig.2 and Table.2 as compared to Cao's algorithm. Obviously, the proposed algorithm can distinguish twice as many signals as Cao's algorithm. Moreover, for the ESPRIT-ID algorithm [13], if two non-overlapping identical subarrays are used, the maximum number of distinguishable signals will be only $\lfloor M/4 \rfloor$. In this case, the proposed algorithm can detect almost four times the number of signals than the ESPRIT-ID.

Table 2: Maximum number of signals distinguished by the two algorithms

Algorithm	Parity of M	Maximum detectable number
Proposed algorithm	odd	$K = M - 1$
	even	$K = M - 1$
Cao's algorithm	odd	$K = (M - 1)/2$
	even	$K = (M - 2)/2$

5. Simulation results

In this part, the effectiveness of the proposed algorithm is evaluated through some simulations as compared to the state-of-the-art techniques, namely Cao's algorithm [21] and the classic ESPRIT-ID [13]. The CRB of the ID noncircular sources is also plotted for reference. Consider that the involved ID noncircular sources emit the BPSK signals, which impinge on the ULA with the adjacent elements spaced half a wavelength apart. The variance of ray-gains is set as $\{\sigma_{\gamma_k}^2\}_{k=1}^K = 1$, and the number of scattering paths is set as $\{L_k\}_{k=1}^K = 100$. We use the root mean square error (RMSE) $RMSE = \sqrt{\frac{1}{KM_c}\sum_{k=1}^{K}\sum_{m=1}^{M_c}\left(\hat{\theta}_{k,m} - \theta_k\right)^2}$ as the performance index, where M_c is the total number of Monte-Carlo trials, $\hat{\theta}_{k,m}$ is the estimate of the central DOA θ_k of the kth signal in the mth Monte-Carlo trial. For the first

simulation, we suppose the total number of ULA sensors is $M = 5$, and the next four simulations, $M = 8$. It should be noted that the number of sensors included in each subarrray is $N = M - 1$ for the proposed algorithm.

In the first simulation, the maximum number of detectable ID signals by the proposed algorithm is studied. According to Remark 2, the maximum number of ID noncircular signals that can be handled by Cao's algorithm is 2 and for the ESPRIT-ID algorithm it is 1, while for the proposed one it is 4. Here, we set the number of ID noncircular signals to 4 with the central DOAs as $\theta_1 = -30^\circ$, $\theta_2 = -5^\circ$, $\theta_3 = 20^\circ$, and $\theta_4 = 40^\circ$. All signals angular distributions are Gaussian with the same angular spread $\sigma = 0.1^\circ$. The SNR is set as 20dB, and the number of snapshots is $T = 200$. Fig.3 shows the resultant spatial spectrum of the proposed algorithm. Obviously, in this case, the proposed one has provided an effective estimation result, while Cao's algorithm and ESPRIT-ID algorithm have failed completely.

In the second simulation, the performance of the proposed algorithm is studied with SNR varying from 0dB to 25dB. There are two uncorrelated ID noncircular signals with the central DOAs $\theta_1 = 30^\circ$ and $\theta_2 = 65^\circ$. Their angular distribution is Gaussian with angular spread $\sigma_1 = 1.5^\circ$ and $\sigma_2 = 1^\circ$. The number of snapshots is 200 and $M_c = 500$. As the number of array sensors is 8, the proposed algorithm divides the array into two 7-sensor subarrays and two 7-sensor extended subarrays as shown in Fig.2(a). However, Cao's algorithm only divides the array into two subarrays with 7 sensors as shown in Fig.2(b). Fig.4 (a) and (b) illustrates the RMSEs of the central DOA estimation and the angular spread estimation for different algorithms, where CRB_n represents the CRB of ID noncircular signals. The CRBs are

also shown as benchmarks. It can be observed that the performance of the proposed algorithm is shown to be superior to Cao's due to the additional noncircularity information exploited. Meanwhile, the ESPRIT-ID algorithm performs poorly in the estimation performance because only a quarter of the sensors is exploited.

In the third simulation, the performance with respect to a varying number of snapshots ranging from 50 to 950 is investigated. The SNR is set at 10dB, the two signals are with the central DOAs $\theta_1 = 10^\circ$ and $\theta_2 = 30^\circ$, their angular distribution is Gaussian with angular spread $\sigma_1 = 2^\circ$ and $\sigma_2 = 1^\circ$, and the other parameters are the same as in the second simulation. As shown in Fig.5 (a) and (b), a similar conclusion can be drawn as in Fig.4, i.e., the proposed algorithm has achieved a better and better performance with the number of snapshots increasing, and again outperformed Cao's algorithm and the ESPRIT-ID algorithm.

In the fourth simulation, the performance of the proposed algorithm is studied versus the angular spread varying from 0.5° to 3°. The SNR is set at 20dB, the angular spread of two uncorrelated ID noncircular signals is set to the same, the central DOAs are set at $\theta_1 = 30^\circ$ and $\theta_2 = 50^\circ$ and the other parameters are the same as in the second simulation. From Fig.6 (a) and (b), it can be seen that as the angular spread increases, the estimated performance of the proposed algorithm and Cao's algorithm [21] becomes worse overall. It can also be observed that the ESPRIT-ID algorithm [13] tends to be stable in general because there are fewer number of ULA sensors utilized. However, with the increase of angular spread, the proposed algorithm still shows better estimation performance than the other two algorithms.

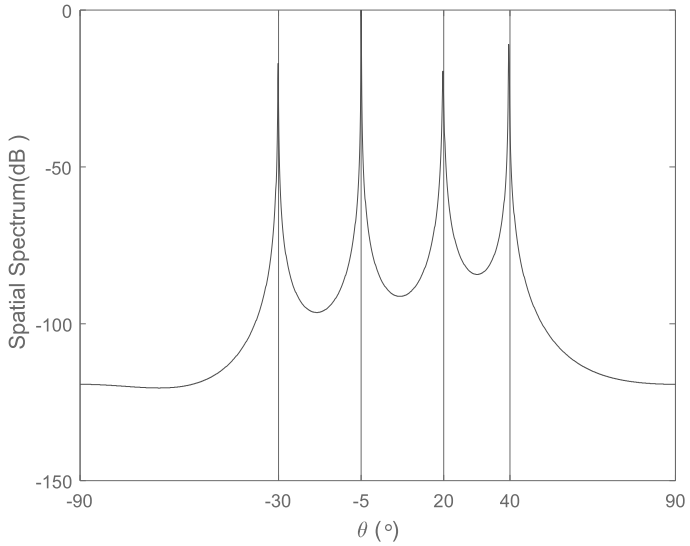

Fig. 3: Spatial spectrum of the proposed algorithm for central DOA estimation.

In the last simulation, in order to examine the applicability of the proposed algorithm to different angular distributions, we consider the case where multiple ID noncircular signals have different angular distributions. Two ID noncircular signals are considered here: one has a central DOA $\theta_1 = 40^\circ$ and exhibits a uniform distribution with $\sigma_1 = 0.5^\circ$, and the other one has a central DOA $\theta_2 = 60^\circ$ and exhibits a Gaussian distribution with $\sigma_2 = 0.7^\circ$. The RMSEs of central DOAs and angular spreads for different algorithms are shown in Fig.7 (a) and (b), respectively. It is shown that the proposed algorithm is still effective in the presence of multiple ID noncircular signals with different angular distributions. In addition, for each type of angular distribution, the proposed algorithm has achieved a more accurate estimation result than Cao's algorithm.

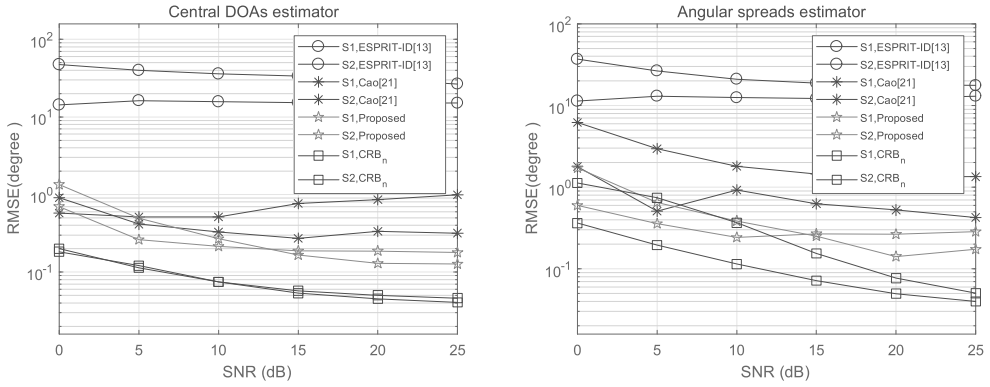

(a) (b)

Fig. 4: RMSE versus SNR for ID noncircular sources. (a) central DOAs. (b) angular spreads.

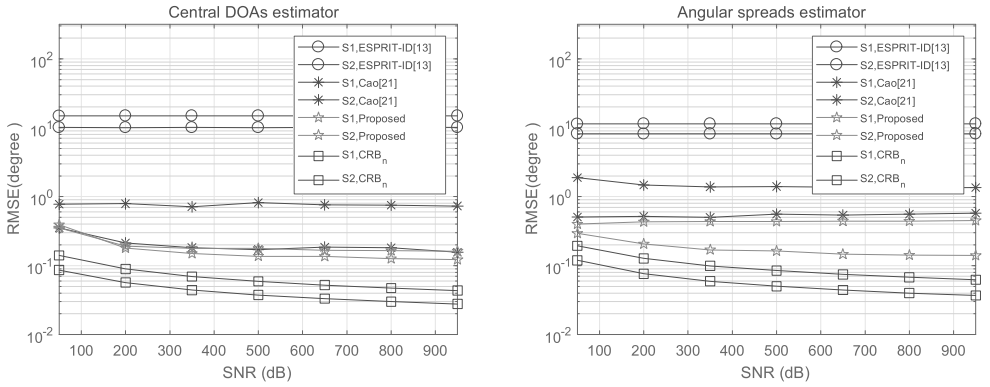

(a) (b)

Fig. 5: RMSE versus number of snapshots for ID noncircular sources. (a) central DOAs. (b) angular spreads.

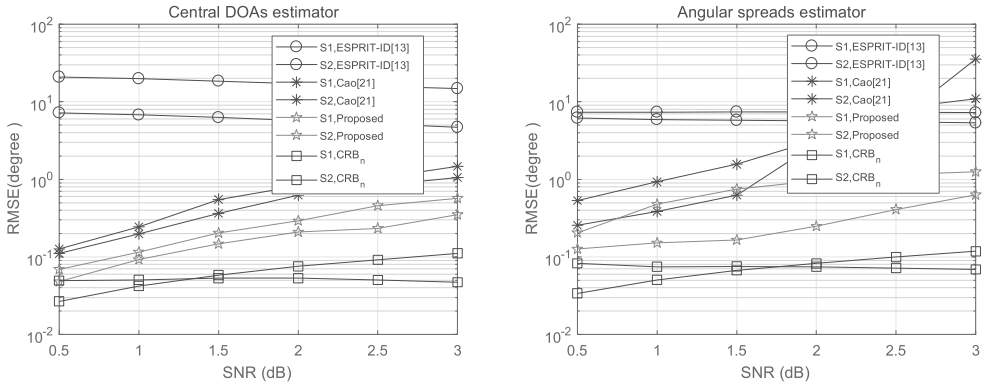

(a) (b)

Fig. 6: RMSE versus angular spread for ID noncircular sources. (a) central DOAs. (b) angular spreads.

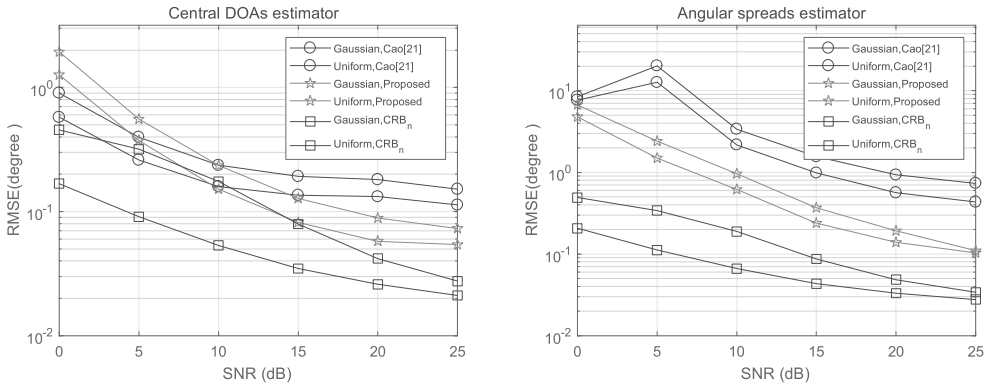

(a) (b)

Fig. 7: RMSE versus SNR with different distributed angular distributions for ID noncircular sources. (a) central DOAs. (b) angular spreads.

6. Conclusion

In this paper, based on the reduced-rank principle, a novel angular parameters estimation algorithm for multiple incoherently distributed noncircular sources has been proposed. By exploiting the noncircularity information of signals and the Taylor series expansion, a generalized rotational invariance relationship based on a ULA structure was obtained for the extended GAMs, with the central DOAs estimated through a spectral peak search. Then, closed-form solutions for angle spreads were estimated by the central moments of the angular distribution and the estimated value of the central DOAs. Also the CRB is analyzed as a benchmark. Compared with the direct 2D spectral peak search algorithm, the proposed one has a much lower computational complexity. Compared to Cao's algorithm and the ESPRIT-ID algorithm, the proposed one can not only improve the estimation accuracy, but also handle more ID noncircular sources, as demonstrated by various simulation results.

Acknowledgement

This work was supported by the National Natural Science Foundation of China under Grants 62001256 and 61871282, and by Key Laboratory of Intelligent Perception and Advanced Control of State Ethnic Affairs Commission under Grant MD-IPAC-2019102, and by Zhejiang Provincial Natural Science Foundation of China under Grants LQ19F010002 and LR20F010001, and by Natural Science Foundation of Ningbo Municipality under Grant 2018A610094, and by the Scientific Research Foundation of Graduate School

of Ningbo University under Grant IF2020112, and by K.C.Wong Magna Fund in Ningbo University.

References

[1] F. Gao, Z. Tian, E. G. Larsson, M. Pesavento and S. Jin, "Introduction to the special issue on array signal processing for angular models in massive MIMO communications," *IEEE J. Sel. Topics Signal Process.*, vol. 13, no. 5, pp. 882-885, Sept. 2019.

[2] F. Wen, J. Shi and Z. Zhang, "Joint 2D-DOD, 2D-DOA and polarization angles estimation for bistatic EMVS-MIMO radar via PARAFAC analysis," *IEEE Trans. Veh. Technol.*, doi: 10.1109/TVT.2019.2957511.

[3] X. Wang, L. Wan, M. Huang, C. Shen and K. Zhang, "Polarization channel estimation for circular and non-circular signals in massive MIMO systems," *IEEE J. Sel. Topics Signal Process.*, vol. 13, no. 5, pp. 1001–1016, Sept. 2019.

[4] Z. Zheng, W. Wang, Y. Kong, and Y. D. Zhang, "MISC array: A new sparse array design achieving increased degrees of freedom and reduced mutual coupling effect," *IEEE Trans. Signal Process.*, vol. 67, no. 7,pp. 1728-1741, Apr. 2019.

[5] H. Chen, W. F. Wang and W. Liu, "Joint DOA, range, and polarization estimation for rectilinear sources with a COLD array," *IEEE Wireless Commun. Lett.*, vol. 8, no. 5, pp. 1398–1401, Sept. 2019.

[6] S. Valaee, B. Champagne and P. Kabal, "Parametric localization of distributed sources," *IEEE Trans. Signal Process.*, vol. 43, no. 9, pp. 2144-2153, Sep. 1995.

[7] M. Ghogho, O. Besson and A. Swami, "Estimation of directions of arrival of multiple scattered sources," *IEEE Trans. Signal Process.*, vol. 49, no. 11, pp. 2467-2480, Nov. 2001.

[8] Z. Zheng, W. Wang, H. Meng, H. C. So and H. Zhang, "Efficient beamspace-based algorithm for two-dimensional DOA estimation of incoherently distributed sources in massive MIMO systems," *IEEE Trans. Veh. Technol.*, vol. 67, no. 12, pp. 11776-11789, Dec. 2018.

[9] Z. Huang, X. Li, P. Huang and W. Wang, "2-D DOA estimation for incoherently distributed sources considering mixed circular and noncircular signals in massive MIMO system," *IEEE Access*, vol. 7, pp. 106900-106911, 2019.

[10] L. Wan, G. Han, J. Jiang, J. J. P. C. Rodrigues, N. Feng and T. Zhu, "DOA estimation for coherently distributed sources considering circular and noncircular signals in massive MIMO systems," *IEEE Syst. J.*, vol. 11, no. 1, pp. 41-49, Mar. 2017.

[11] R. Schmidt, "Multiple emitter location and signal parameter estimation," *IEEE Trans. Antennas Propag.*, vol. 34, no. 3, pp. 276-280, Mar. 1986.

[12] R. Roy and T. Kailath, "ESPRIT-estimation of signal parameters via

rotational invariance techniques," *IEEE Trans. Acoust., Speech, Signal Process.*, vol. 37, no. 7, pp. 984-995, Jul. 1989.

[13] S. Shahbazpanahi, S. Valaee and M. Bastani, "Distributed source localization using esprit algorithm," *IEEE Trans. Signal Process.*, vol. 49, no. 10, pp. 2169-2178, Oct. 2001.

[14] A. Zoubir and Y. Wang, "Efficient DSPE algorithm for estimating the angular parameters of coherently distributed sources," *Signal Process.*, vol. 88, no. 4, pp. 1071-1078, Apr. 2008.

[15] W. Y. Chen, X. F. Zhang, L. Xu and Q. L. Cheng, "Successive DSPE-based coherently distributed sources parameters estimation for unmanned aerial vehicle equipped with antennas array," *Phys. Commun.*, vol. 32, pp. 96-103, 2019.

[16] W. M. Xiong, J. Picheral and S. Marcos, "Performance analysis of distributed source parameter estimator (DSPE) in the presence of modeling errors due to the spatial distributions of sources," *Signal Process.*, vol. 143, pp. 146-151, Feb. 2018.

[17] J. A. Chaaya, J. Picheral and S. Marcos, "Localization of spatially distributed near-field sources with unknown angular spread shape," *Signal Process.*, vol. 106, pp. 259-165, Jan. 2015.

[18] Y. Meng, P. Stoica and K. Wong, "Estimation of the directions of arrival of spatially dispersed signals in array processing, " *IEE Proc. Radar Sonar Navig.*, vol. 143, no. 1, pp. 1-9, Feb. 1996.

[19] O. Besson and P. Stoica, "Computationally efficient maximum likelihood approach to DOA estimation of a scattered source," *Wireless Pers. Commun.*, vol. 16, no. 2, pp. 135-148, 2001.

[20] S. Shahbazpanahi, S. Valaee and A. B. Gershman, "A covariance fitting approach to parametric localization of multiple incoherently distributed sources," *IEEE Trans. Signal Process.*, vol. 52, no. 3, pp. 592-600, Mar. 2004.

[21] R. Z. Cao, F. F. Gao and X. F. Zhang, "An angular parameter estimation method for incoherently distributed sources via generalized shift invariance," *IEEE Trans. Signal Process.*, vol. 64, no. 17, pp. 4493-4503, Sept 2016.

[22] Z. Zheng, J. Lu, W. Q. Wang, H. F. Yang and S. S. Zhang, "An efficient method for angular parameter estimation of incoherently distributed sources via beamspace shift invariance," *Digit. Signal Process.*, vol. 83, pp. 261-270, 2018.

[23] J. Zhuang, H. Xiong, W. Wang and Z. Chen, "Application of manifold separation to parametric localization for incoherently distributed sources, " *IEEE Trans. Signal Process.*, vol. 66, no. 11, pp. 2849-2860, June. 2018.

[24] S. B. Hassen, F. Bellili, A. Samet and S. Affes, "Angular parameters estimation of multiple incoherently distributed sources generating non-circular signals," *IEEE Access*, vol. 7, pp. 38451-38468, 2019.

[25] Y. L. Huang, Y. G. Xu, Y. Lu and Z. W. Liu, "Aligned propagator scanning approach to DOA estimation of circular and noncircular wideband source signals," *IEEE Trans. Veh. Technol.*, vol. 68, no. 2, pp. 1702-1717, Feb 2019.

[26] H. Chen, Y. Liu, Q. Wang, W. Liu and G. Wang, "Two-dimensional angular parameter estimation for noncircular incoherently distributed sources based on an L-shaped array," *IEEE Sensors J.*, doi: 10.1109/JSEN.2020.3006431.

[27] H. Chen, C. P. Hou, W. P. Zhu, W. Liu, Y. Y. Dong, Z. J. Peng and Q. Wang, "ESPRIT-like two-dimensional direction finding for mixed circular and strictly noncircular sources based on joint diagonalization," *Signal Process.*, vol. 141, pp. 48-56, Dec 2017.

[28] X. M. Yang, G. J. Li, C. C. Ko, Z. Zheng and T. S. Yeo, "Central DOA estimation of incoherently distributed noncircular sources with cross-correlation matrix," *Circuits Syst. Signal Process.*, vol. 34, pp. 3697-3707, 2015.

[29] X. Yang, Z. Zheng and B. Hu, "Off-grid DOA estimation of incoherently distributed non-circular sources via generalised approximate message passing," *Electron. Lett.*, vol. 52, no. 4, pp. 262-264, Jan. 2016.

[30] Z. L. Dai, B. Ba, W. J. Cui, and Y. M. Sun, "Computational efficient two-dimension DOA estimation for incoherently distributed noncircular sources with automatic pairing," *IEEE Access*, Oct. 2017.